AJNR

Comparison of xenon-enhanced CT with ultrafast CT for measurement of regional cerebral blood flow.

G T Gobbel, C E Cann and J R Fike

AJNR Am J Neuroradiol 1993, 14 (3) 543-550
http://www.ajnr.org/content/14/3/543

Comparison of Xenon-Enhanced CT with Ultrafast CT for Measurement of Regional Cerebral Blood Flow

Glenn T. Gobbel,[1,2,4] Christopher E. Cann,[3] and John R. Fike[1-3]

PURPOSE: To compare an ultrafast CT method for estimating regional cerebral blood flow with a more commonly used xenon-enhanced CT method. **METHODS:** Xenon CT and ultrafast CT were used to estimate regional cerebral blood flow (rCBF) in 12 healthy beagle dogs. Measurements were obtained for left and right hemisphere, cortical gray matter, basal ganglia, and deep white matter. The ability of each method to show differences in blood flow between regions of high flow (gray matter) and low flow (white matter) was evaluated, both for large (>0.75 cm^3) and small (<0.5 cm^3) regions of interest. In addition, side-to-side differences in rCBF were evaluated to determine the minimum difference that would suggest a significant alteration in blood flow. **RESULTS:** There was less interanimal variance in absolute rCBF measurements obtained using xenon CT; ultrafast CT appeared to accentuate rCBF differences between high flow and low flow regions. There were strong side-to-side correlations in rCBF when measured by ultrafast CT, which suggests that this technique may be particularly useful in detecting focal alterations in rCBF restricted to one hemisphere of the brain. **CONCLUSIONS:** Ultrafast CT measures of rCBF compare favorably with those obtained using xenon CT.

Index terms: Cerebral blood, flow; Blood, flow dynamics; Computed tomography, comparative studies; Brain, computed tomography; Animal studies

AJNR 14:543–550, May/Jun 1993

Noninvasive measurement of regional cerebral blood flow (rCBF) has important applications in the assessment and management of patients with a wide variety of neurologic conditions (1–9). Some clinical situations, such as brain death or global ischemic injury, require that the measurements made be compared directly with a normal range. Such areas are typically large, comprising major regions or even entire hemispheres of the brain. In contrast, in other abnormalities, such as brain tumors, arteriovenous malformations, acute infarctions, or radiation injury, alterations in blood flow may be focal and heterogeneous in nature, with regions of both increased and decreased flow relative to normal brain. To detect changes in rCBF under the latter conditions, it would be useful to be able to measure rCBF in relatively small regions of interest (ROIs). The accuracy and sensitivity required of techniques used to measure rCBF may differ depending upon the type of measurement desired (eg, global vs focal). In the present study, we used an ultrafast computed tomographic (CT) method that recently has been shown to be useful for estimating rCBF in localized regions of the brain such as the basal ganglia (10). Regional CBF values measured using this technique were compared with those obtained using a more commonly used CT method, xenon-enhanced CT (xenon CT).

Rapid sequence or dynamic CT for estimation of blood flow requires that a rapid series of CT scans be obtained after an intravenous bolus of iodinated contrast material (11). Ultrafast CT differs from previous dynamic CT methods by its ability to obtain a 100 msec "snapshot" image of the iodine content in the brain at a frequency greater than one per second. Ultrafast CT thus makes it possible to obtain accurate contrast concentration versus time curves as the contrast

Received September 24, 1991; revision requested December 24; revision received June 22, 1992 and accepted August 31.

This study was supported by NIH grants CA 13525 and CA 09215 and a gift from the Phi Beta Psi Sorority.

[1] Brain Tumor Research Center, Department Neurological Surgery, Departments of [2]Radiation Oncology and [3]Radiology, and [4]Graduate Group in Biophysics, School of Medicine, University of California, San Francisco, CA 94143. Address reprint requests to John R. Fike, Ph.D., Box 0520, HSW 783, University of California, San Francisco, CA 94143.

AJNR 14:543–550, May/Jun 1993 0195-6108/93/1403–0543

passes through the brain. These time-concentration curves can then be analyzed to quantify rCBF accurately (10). In addition, other parameters relating to rCBF, including mean transit time and vascular volume, can be derived from the ultrafast CT data (10, 12).

Other noninvasive methods of rCBF measurement have been developed, including xenon CT, positron emission tomography, and single photon emission CT. While debate exists over the relative merits of these methods, xenon CT has become a commonly used technique because it is commercially available for a number of CT scanners and relatively easy to implement. Furthermore, xenon CT does not require dedicated instrumentation or special isotope production facilities as does positron emission tomography. Xenon CT generally provides better spatial resolution than the other widely available method, single photon emission computed tomography (13), and regions of interest (ROIs) on the order of 1 cm^3 give rCBF results reproducible to about 12% (3). We have used ultrafast CT and xenon CT to measure regional differences in CBF in normal adult beagle dogs. The ability of each method to detect differences in blood flow between regions of high flow (gray matter) and low flow (white matter) was evaluated, both for large (>0.75 cm^3) and small (<0.5 cm^3) ROIs. In addition, side-to-side differences in rCBF were evaluated to determine the minimum difference that would suggest a significant alteration in blood flow.

Methods

Animals and Preparation

Six male and six female purebred adult beagle dogs, varying in age from 9 to 32 months, were purchased from a commercial supplier. In accordance with National Institutes of Health guidelines for care and handling of laboratory animals, all animals were housed under standardized conditions and given routine veterinary care.

Dogs were anesthetized for all procedures. Preanesthetics included 0.05 mg/kg of atropine sulfate and 0.25 mg/kg of acepromazine maleate administered subcutaneously 20 to 30 minutes before induction. General anesthesia was induced with sodium thiamylal (4% to effect) given intravenously through an 18-gauge catheter placed in a cephalic vein. Following intubation, general anesthesia was maintained with periodic intravenous boluses of sodium thiamylal.

Xenon CT

A GE 9800 CT scanner outfitted with a GE xenon blood flow imaging system (General Electric Medical Systems, Milwaukee, WI) was used in all studies. Dogs were placed in sternal recumbency with the head extended onto a plastic head rest within the CT scanner. To maximize the reproducibility of xenon uptake curves, the endotracheal tube was connected to a Harvard respirator set at 200 ml tidal volume and 16 breaths per minute. The xenon administration tank was then connected to the inflow valve of the respirator. The xenon gas mixture was nominally 31% xenon and 0.6% to 0.8% CO_2, with the balance O_2; the CO_2 in the mixture was designed to stabilize respiration and thus optimize the calculation of the arterial input function.

A lateral computed radiograph was taken of the skull, and transverse CT scans of the brain were obtained for localization of the desired scan plane. The scan level just rostral to the thalamus was chosen for the xenon CT study. Scanning parameters were 80 KVp and 200 mA with a 4-second scan time; scan thickness was 5 mm. Two baseline scans were obtained prior to the inhalation of xenon, and six scans were obtained over a 6-minute period after the start of xenon inhalation. Expired xenon concentration was monitored by the system and used to calculate the arterial input function as described in detail elsewhere (14). A venous blood sample was obtained for hematocrit determination as required by the GE xenon system. Images were reconstructed on a 256 × 256 matrix with a pixel size of 0.5 mm.

Xenon CT studies preceded the ultrafast CT studies in all but one dog, and at least 48 hours elapsed between the two examinations.

Ultrafast CT

All studies were done using an ultrafast CT scanner (C-100XL, Imatron Inc., South San Francisco, CA). Placement of the animals within the scanner and determination of scanning level were the same as for the xenon CT study. Ventilation was also the same, except that room air was used in place of the xenon gas mixture.

A 15-ml bolus of iodinated contrast (Na/meglumine-iothalamate, Conray 400®, iodine content: 400 mg/ml, Mallinckrodt, Inc., St. Louis, MO), timed to begin with the first in a series of 20 CT scans (Fig. 1), was injected into the cephalic vein catheter at a rate of 5 mL/sec using a mechanical injector (Medrad, Mark IV, Pittsburgh, PA). The CT scans, each scan 6-mm thick, were obtained using a scan duration of 0.1 seconds and an interscan delay of 0.8 seconds. Scans were done at 130 KVp and exposures were 63 mAs. Images were reconstructed on a 360 × 360 matrix; pixel size was 0.5 mm.

Data Analysis

Following the xenon flow study, the system software smoothed all the images to reduce pixel noise, averaged the two baseline CT scans, and subtracted the resulting pixel density from each of the post-xenon inhalation scans on a pixel-by-pixel basis to determine the xenon enhancement as a function of time. By combining the pixel en-

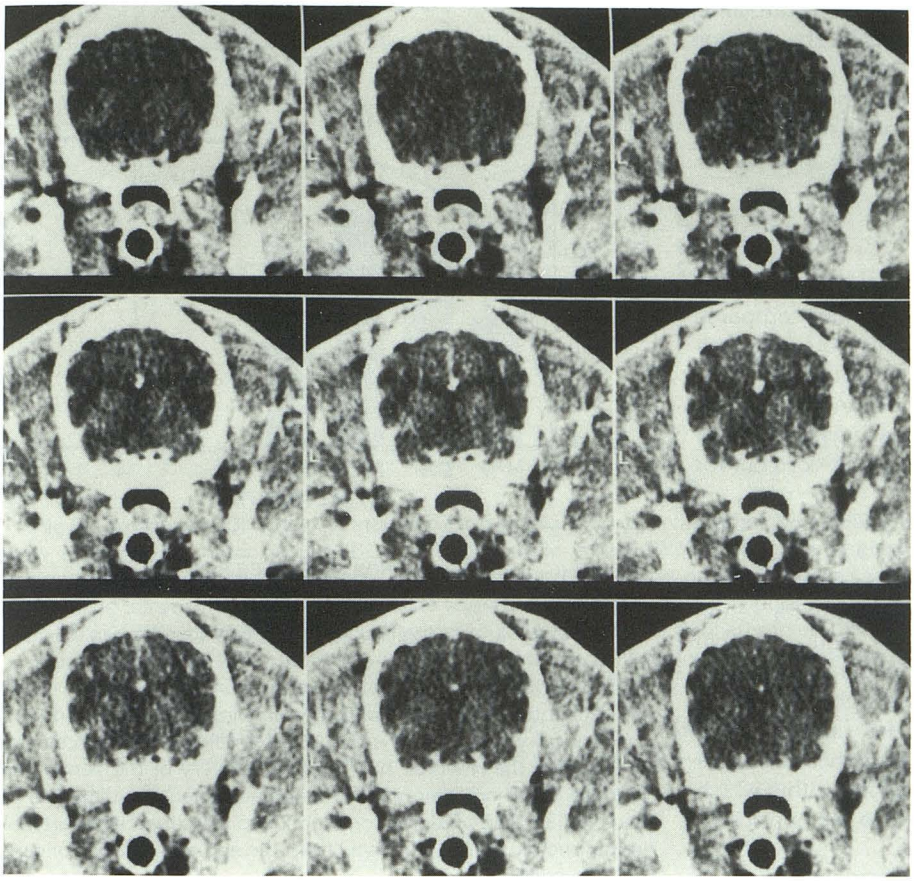

Fig. 1. Transverse ultrafast CT images of dog brain during the passage of a 15-ml bolus of iodinated contrast medium. The images represent nine of the 20 images obtained every 0.8 seconds. The top three images were obtained prior to arrival of the bolus, the middle images near the peak of contrast enhancement, and the bottom images during contrast washout. A focal lesion resulting from ^{125}I irradiation can be seen in the upper right quadrant of the brain. Images are viewed looking rostrally, with the right side of the head to the viewer's right.

hancement data with the end-tidal xenon concentration data, rCBF values were derived for each CT image pixel according to methods described previously in detail (3). A functional perfusion image of the brain, in which the gray scale represented the rCBF values within each voxel, was generated from these data. Original scans and computed xenon images were converted to a standard file format and transferred to a specially programmed offline computer system for analysis.

Irregular ROIs, labeled as cortical gray matter, basal ganglia, deep white matter, and hemisphere, were drawn on a single CT image using a manually directed, trackball-guided cursor as described previously (10). The volumes (mean ± standard error) of the ROIs used in data analysis of the xenon CT studies were 2.36 ± 0.06 cm^3 for the hemisphere, 0.76 ± 0.16 cm^3 for the cortical gray matter, 0.30 ± 0.01 cm^3 for the basal ganglia, and 0.33 ± 0.01 cm^3 for the deep white matter. The gray matter, white matter, and basal ganglia ROIs largely contained the desired tissue components, although some inclusion of surrounding tissues was unavoidable. The ROI size and placement were based on previous anatomical studies (15, 16). Each ROI was then mapped onto the corresponding location on the functional perfusion image, and the average rCBF was recorded.

Following the ultrafast CT study, a manually directed, trackball-guided cursor was used to outline ROIs corresponding to those used in the xenon CT studies, ROI volumes were 2.27 ± 0.09, 1.23 ± 0.06, 0.35 ± 0.01, and 0.40 ± 0.01 cm^3 for the hemisphere, cortical gray matter, basal ganglia, and deep white matter, respectively. The ROIs were drawn on a single CT scan as described previously (10), and the average CT number for the same ROI on each of the 20 scans was computed by the scanner software. Because changes in CT number from baseline following the administration of contrast agent are linearly related to the amount of contrast agent within the tissue (17), ROI CT number versus time data correspond directly to ROI contrast concentration versus time curves.

A gamma-variate time-concentration curve was then fit to the data using the least-squares procedure of the scanner software. The gamma-variate curve has been shown to approximate closely a time-concentration curve without recirculation (18). Parameters of the fitted curve, including area under the curve (AUC) and center of gravity of the curve ($<t>$) were automatically displayed adjacent to the CT image. Center of gravity represents the mean position of the gamma variate function relative to time (18). The curve parameters for an arterial (ART) ROI and for each brain region were then combined to derive rCBF estimates according to previously derived equations (10, 12, 19):

$$rCBF = \text{vascular volume}/\text{mean transit time}$$

$$\text{vascular volume} = AUC_{ROI}/AUC_{ART}$$

$$\text{mean transit time} = <t_{ROI}> - <t_{ART}>.$$

Vascular volume refers to the fraction of a region containing flowing blood and mean transit time refers to the average time required for a single molecule within the blood to traverse the region. The single pixel within the left or right lingual artery with the greatest increase in CT number from baseline was used for determination of the arterial CT number versus time data (10).

Statistical Analysis

The rCBF within each of the eight ROIs was compared with the rCBF within every other ROI. Separate comparisons were carried out for the two methods of rCBF determination. Differences in rCBF were evaluated for significance using a single-factor repeated-measures analysis of variance followed by a Scheffe *F* test, which corrects for multiple comparisons (20).

The relationship between absolute rCBF values on the left and right sides within the various ROIs was determined using simple correlation and paired left-right differences. Left-right comparisons were done independently for xenon CT and ultrafast CT, but all regions were grouped within each modality for determination of confidence intervals. The 95% confidence intervals for the left-right differences within the lower quartile, middle 50%, and upper quartile of the range of blood flows were determined; these intervals were defined as the range of normal variability within which side-to-side differences were considered to be nonsignificant.

Xenon CT and ultrafast CT rCBF determinations were considered to be independent modalities. However, for descriptive purposes only, rCBF measured by ultrafast CT and xenon CT in each ROI in each individual was compared, and the differences for each region were tested using a paired *t* test. Significance was assigned at the 0.05 level.

Results

Under our experimental conditions, smooth and reproducible xenon uptake data were obtained (Fig. 2).

Average rCBF values in the four ROIs are shown in Figure 3, and for a given ROI, the range of values is wider when measured by ultrafast CT. Ultrafast CT detected significantly lower rCBF in the deep white matter relative to the cortical gray matter, basal ganglia, and whole hemisphere for individual animals. When rCBF was measured using xenon CT, rCBF in white matter was not consistently lower than within regions of gray matter or in mixed gray/white matter (hemisphere); that is, there was no significant difference between left deep white matter and right cortical gray matter, left hemisphere, or right hemisphere. Neither technique detected significant differences in blood flow between the cortical gray matter and basal ganglia. Ultrafast

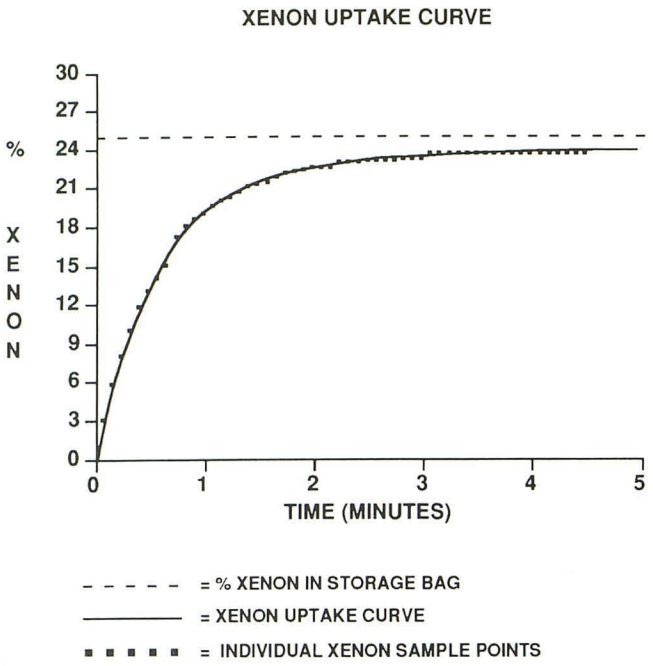

Fig. 2. Xenon uptake curve (xenon concentration in expired air versus time after start of xenon inspiration) obtained during mechanical ventilation. The dashed line indicates the percentage of xenon in the reservoir bag used for delivery of the xenon gas mixture. Each dot represents the actual percentage of xenon in end-tidal air. The solid line corresponds to the curve of the arterial input function, which is derived from the end-tidal xenon concentration versus time data.

CT rCBF values tended to be higher than those measured by xenon CT for all the ROIs, but the only significantly higher values were those measured within the right neocortex and hemisphere (paired *t* test).

Left-right comparisons showed a highly significant relationship for ultrafast CT when all ROIs were combined ($r = .96$, Fig. 4). For xenon CT, the correlation between left and right side rCBF was lower ($r = .55$). Left-right differences for the lower quartile (23–48 mL/100 mL/min), middle 50% (49–100 mL/100 mL/min), and upper quartile (101–219 mL/100 mL/min) of the range of blood flows measured by ultrafast CT were −0.6 ± 14.5, −0.7 ± 23.5, and 3.2 ± 43.9 mL/100 mL/min, respectively (mean difference ±95% confidence limits). Left-right differences for the lower quartile (38–49 mL/100 mL/min) and middle 50% (50–69 mL/100 mL/min) of the range of blood flows measured by xenon CT were 11.3 ± 26.5 and 6.0 ± 26.6, respectively. The left-right difference for the upper quartile (70–81 mL/100 mL/min) for the range was 2.7 ± 21.1 and was lower than the difference measured by ultrafast CT.

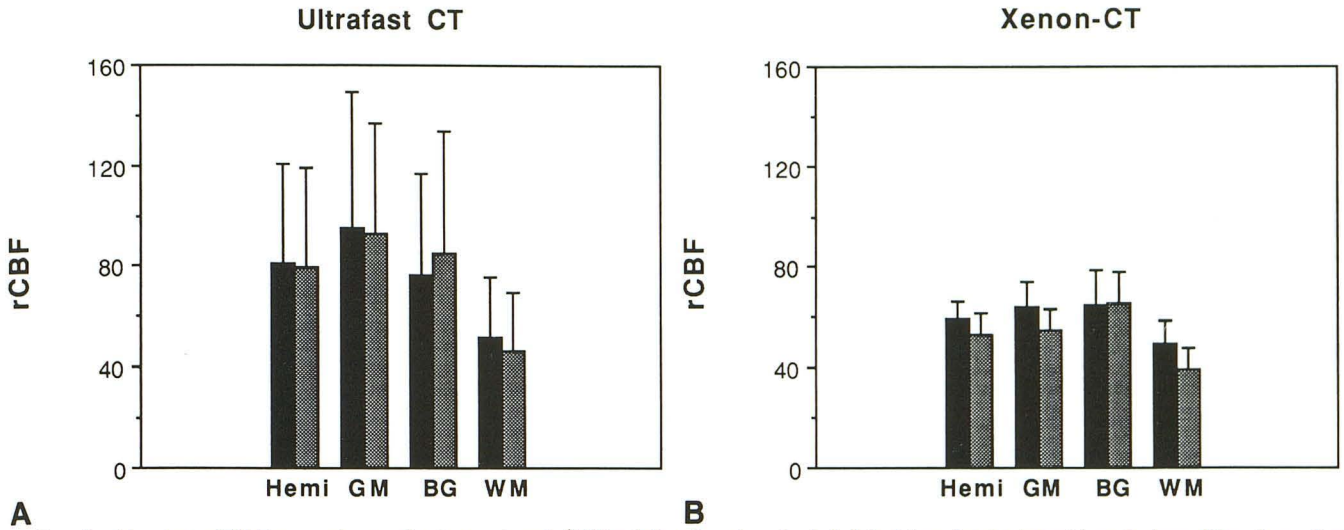

Fig. 3. Absolute rCBF (mean ± standard error in mL/100 mL/min) within the left (black) and right (gray) hemisphere (Hemi), cortical gray matter (GM), basal ganglia (BG), and deep white matter (WM) ROIs as determined using ultrafast CT (*A*) and xenon CT (*B*) techniques. Although there is greater variance in the rCBF values determined using ultrafast CT, this technique detected significant differences between the pure white matter regions (deep white matter) and pure gray matter regions (cortical gray matter and basal ganglia) as well as between pure white matter regions and both hemispheres in all cases. With xenon CT, rCBF in white matter regions was not consistently lower than that within gray matter regions and within hemispheres.

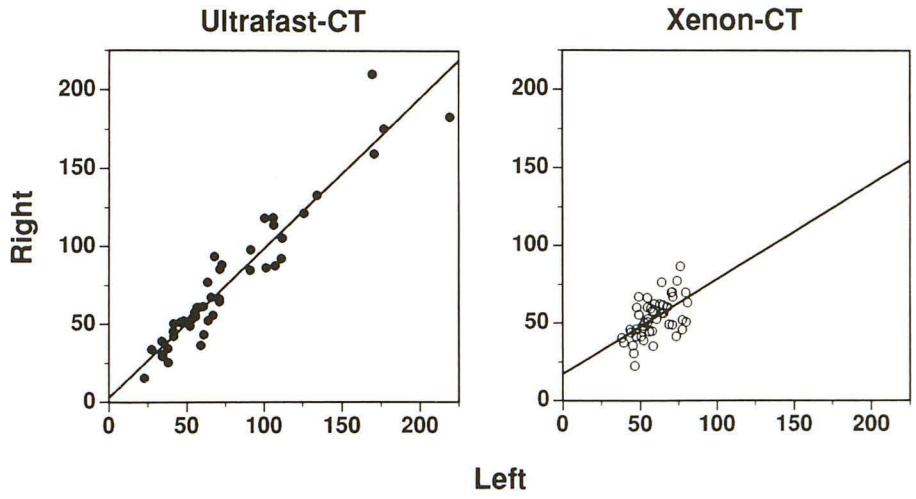

Fig. 4. Comparison of left- and right-sided rCBF (mL/100 mL/min) for all ROIs studied using ultrafast CT (left) and xenon CT (right). The data were fit using simple regression analysis, and the least squares line of regression is shown on each graph. Correlation coefficients were .96 and .55 for ultrafast CT and xenon CT respectively.

Discussion

Xenon CT has been used extensively in the evaluation of normal and pathologic tissues in humans and animals, and is an accepted method to determine perfusion values under a variety of clinical and experimental situations (2–4, 21). Perfusion estimates obtained using xenon CT have been compared with rCBF determined with radioactive microspheres, and there was a significant association between the results from the two procedures (22–24). Furthermore, the xenon CT methodology provides a measure of brain partition coefficients, which have been shown to change under pathologic conditions (25). However, there are some limitations to this technology, including examination time, which requires that the patient lie perfectly still for at least 6 minutes, and radiation dose (~8 cGy (3)). In addition, breathing the xenon gas mixture can lead to alterations in respiratory rate and an erratic xenon uptake curve due to both the anesthetic effects of xenon and the fall in blood CO_2 levels accompanying the inhalation of a CO_2-free gas. Scanning protocols that emphasize data acquired during the early phase of xenon inhalation may help reduce this effect (3). To minimize the effects of xenon on respiratory rate in the present study, we standardized our xenon scanning protocol by adding CO_2 to the xenon gas mixture (3) and by mechanically ventilating the animals. It

was our goal to employ this optimized xenon procedure and to compare the rCBF estimates obtained using xenon CT with those obtained using ultrafast CT.

Previous attempts to examine rCBF with dynamic CT were limited to a qualitative assessment of concentration-versus-time curves or the determination of rCBF-related parameters, such as the center of gravity of the CT number-versus-time curves (26–29). The development of the ultrafast CT scanner with scan acquisition times of 50 to 100 msec (30) and a modification of methods (10, 12) first proposed by Axel (19) has made it possible to extend the capabilities of dynamic CT to quantify rCBF. Comparison of ultrafast CT estimates of rCBF with estimates obtained using the radiolabeled microsphere method has shown a strong correlation ($r = .95$) between the two methods for ROIs as small as 0.3 to 0.4 cm^3, and over a wide range of pCO_2 values; blood flow measured by these techniques ranged from 12 mL/100 g/min in the internal capsule to 168 mL/100 g/min in the neocortex (10). There was also good agreement between the microsphere and ultrafast CT estimates of reduced rCBF in regions of brain damaged by focal irradiation (10).

In the present study, the absolute rCBF values determined using ultrafast CT varied over a wider range than those determined using xenon CT and tended to be higher on average (Fig. 3). Ultrafast CT-derived values for deep white matter averaged 45–50 mL/100 g/min and values for individual animals ranged from a low of 15 to a high of 106. Xenon CT values for the same ROI also averaged about 45 mL/100 g/min, but ranged from a low of 22 to a high of 73. Even in relatively high blood flow tissues such as cortical gray matter and basal ganglia, the range of xenon CT rCBF was about 40 to 85 mL/100 g/min. In contrast, the range of rCBF in the gray matter ROIs as determined by ultrafast CT rCBF ranged from 40 to 210 mL/100 g/min.

There are a number of factors that may be responsible for the differences in measured rCBF values between the two techniques used here. Perhaps most important are the fundamental distinction between the two methods. The ultrafast CT technique measures the passage of nondiffusible contrast medium as it flows through the vasculature of the brain. On the other hand, xenon CT measures the accumulation of a freely diffusible gas in tissue, a process that is diffusion limited. Tomita and Gotoh (31) considered the use of diffusible tracers for measurement of rCBF and indicated that in high flow situations, those measurements could underestimate actual rCBF values. Furthermore, ultrafast CT may overestimate rCBF under conditions of high flow and short mean transit time (10, 12). In the present study, absolute measures within relatively low flow regions such as white matter were similar in the two techniques (Fig. 3); much larger differences were observed in the higher flow areas of gray matter, basal ganglia, and hemisphere. It is likely that the potential underestimation of high rCBF by xenon CT (31) and overestimation of high rCBF by ultrafast CT (10, 12) are responsible for the observed differences.

The differences in absolute rCBF may also be related to hemodynamic alterations induced by the iodinated contrast agent used in the ultrafast CT studies, inasmuch as such agents have established vasoactive effects (32, 33). The xenon/CO_2/O_2 gas mixture used in the xenon CT studies may also contribute the observed differences between the techniques. However, xenon gas has generally been reported to increase rCBF, so effects of the gas would not explain the lower absolute values or the smaller range of rCBF values measured here. Alternatively, the data-smoothing algorithm employed by the image processing software could reduce the range of rCBF values determined by xenon CT (23).

Ultrafast CT consistently detected differences in blood flow between gray and white matter. Invasive measurements of rCBF within normal white and gray matter have demonstrated repeatedly that blood flow within the white matter regions is typically one fourth to one half that of gray matter (34); our ultrafast CT results are in agreement with that study. While xenon CT did detect regional differences in blood flow between white and gray matter in most cases, it did not detect such differences consistently. Of the 12 comparisons of deep white matter with gray matter or regions of mixed tissue (hemisphere), three showed no significant difference in rCBF.

In our study, we were restricted to a minimum scan thickness of 5 mm for the xenon CT study, and we selected the most comparable scan thickness available for the ultrafast CT study, 6 mm. Because the scan thickness used for the two methods differed, the volumes of tissue sampled were also different, and it is possible that this could account, at least in part, for the disparity in sensitivity of the two methods to determine differences in rCBF. Because small ROIs sample minimal amounts of tissue, there is a greater

uncertainty in the CT numbers because of image noise, and thus there is greater uncertainty in the rCBF values derived from changes in those CT numbers. Gur et al (35) considered the relative errors of xenon rCBF values as a function of ROI size and estimated that for small ROIs such as those used here, the error would be 30% or less. Estimations of precision (standard deviation of the percent differences between true and calculated rCBF values) based on simulated ultrafast CT data (Gobbel et al, unpublished) suggested that for small ROIs, the precision was also 30% or less. Larger ROIs would reduce these measurement errors, but larger sample volumes taken from thicker scans may lead to more averaging of gray and white matter within an ROI selected to be pure gray or white matter. Although these considerations may have impacted our study, it seems unlikely that ROI volume alone can explain the observed differences in sensitivity of the two methods to detect differences in rCBF.

The strong side-to-side correlations provided by ultrafast CT of blood flow in normal brain (Fig. 4) would be of particular use for those situations in which lesions are of a focal nature, such as some brain tumors, cerebral infarcts, radiation-induced brain injury, or arteriovenous malformations, particularly at flows less than 100 mL/100 mL/min. Any alteration in rCBF that was confined to one hemisphere would likely be detected provided that the side-to-side difference exceeded the range of differences measured in normal brain.

The present data indicate that ultrafast CT may offer an alternative CT method for the determination of rCBF. Using this method, up to four levels of the brain can be scanned simultaneously in a period of approximately 30 seconds. Additional levels can then be immediately acquired with further boluses of contrast, with the only limitations being the dose of contrast and the dose of radiation, which is about 3 to 4 cGy per flow study. In addition, other hemodynamic information can be determined in addition to rCBF, including mean transit time and vascular volume. These endpoints have been used effectively in the quantitative assessment of experimentally induced focal lesions in dog brain (36, 37). Finally, there are good correlations of ultrafast CT and microsphere estimates of rCBF using ROIs appreciably smaller than those typically used with other noninvasive techniques (3, 10). On the other hand, the ultrafast CT manufacturer has not yet provided functional flow images of the brain as does the xenon software, necessitating operator-directed analysis and selection of ROIs. However, functional images have been generated using other dynamic CT data, and rCBF images can be generated from ultrafast CT data using similar algorithms.

Ultrafast CT measures of rCBF compare favorably with those obtained using xenon CT. The two methods measure different phenomena relating to blood flow and each has advantages and disadvantages. Xenon CT has already been shown to be clinically useful and future clinical trials using ultrafast CT will determine whether this method will also have a clinical impact. Ultrafast CT, with its ability to measure rCBF in relatively small ROIs and its high level of side-to-side correlation in rCBF, should be a useful new tool in the study and evaluation of cerebral blood flow.

Acknowledgment

We would like to thank Liv Cann and Theresa Seilhan for technical assistance.

References

1. Ashwal S, Schneider S, Thompson J. Xenon computed tomography measuring cerebral blood flow in the determination of brain death in children. *Ann Neurol* 1989;25:539–546
2. Yonas H, Sekhar L, Johnson DW, Gur D. Determination of irreversible ischemia by xenon-enhanced computed tomographic monitoring of cerebral blood flow in patients with symptomatic vasospasm. *Neurosurgery* 1989;24:268–372
3. Yonas H, Gur D, Latchaw R, Wolfson SK. Stable xenon CT/CBF imaging: laboratory and clinical experience. *Adv Tech Stand Neurosurg* 1987;15:3–37
4. Hughes RL, Yonas H, Gur D, Latchaw R. Cerebral blood flow determination within the first 8 hours of cerebral infarction using stable xenon-enhanced computed tomography. *Stroke* 1989;20:754–760
5. Chollet F, Celsis P, Clanet M, Guiraud-Chaumeil B, Rascol A, Marc-Vergnes J. SPECT study of cerebral blood flow reactivity after acetazolamide in patients with transient ischemic attacks. *Stroke* 1989;20:458–464
6. Cohan SL, Mun SK, Petite J, Correia J, Da Silva AT, Waldhorn RE. Cerebral blood flow in humans following resuscitation from cardiac arrest. *Stroke* 1989;20:761–765
7. Jinkins JR. Dynamic CT of micro- and macroangiopathic states of the cerebrum. *Neuroradiology* 1988;30:22–30
8. Jinkins JR. Neoplastic encephalopathy: dynamic CT of cerebral gliomata. *Neuroradiology* 1988;30:408–420
9. Hawkins RA, Phelps ME. PET in clinical oncology. *Cancer Metastasis Rev* 1988;7:119–142
10. Gobbel GT, Cann CE, Iwamoto HS, Fike JR. Measurement of regional cerebral blood flow using ultrafast computed tomography: experimental validation. *Stroke* 1991;22:772–779
11. Jaschke WR, Gould RG, Cogan MG, Sievers R, Lipton MJ. Cine-CT measurement of cortical renal blood flow. *J Comput Assist Tomogr* 1987;11:779–784

12. Gobbel GT, Cann CE, Fike JR. Measurement of regional cerebral blood flow using ultrafast computed tomography: theoretical aspects. *Stroke* 1991;22:768–771
13. Meyer JS, Shinohara T, Imai A, et al. Imaging local cerebral blood flow by xenon-enhanced computed tomography—technical optimization procedures. *Neuroradiology* 1988;30:283–292
14. Yonas H, Wolfson SK, Gur D, et al. Clinical experience with the use of xenon-enhanced CT blood flow mapping in cerebral vascular disease. *Stroke* 1984;15:443–450
15. Kaufman HH, Cohen G, Glass TF, et al. CT atlas of the dog brain. *J Comput Assist Tomogr* 1981;5:529–537
16. Zook BS, Hitzelberg RA, Fike JR, Bradley EW. Anatomy of the beagle in cross-section: head and neck. *Am J Vet Res* 1981;42:844–849
17. Jaschke W, Gould RG, Assimakopoulos PA, Lipton MJ. Flow measurements with a high-speed computed tomography scanner. *Med Phys* 1987;14:238–243
18. Thompson HK, Starmer F, Whalen RE, McIntosh HD. Indicator transit time considered as a gamma variate. *Circ Res* 1964;14–502–515
19. Axel L. Cerebral blood flow determination by rapid sequence scanning. *Radiology* 1980;137:679–686
20. Devore J. *Probability and statistics for engineering and the sciences.* Monterey, CA: Brooks/Cole, 1987:391
21. Yonas H, Gur D, Claasen D, Wolfson SK, Moossy J. Stable xenon enhanced computed tomography in the study of clinical and pathologic correlates of focal ischemia in baboons. *Stroke* 1988;19:228–238
22. Dewitt DS, Fatouros PP, Wist AO, et al. Stable xenon versus radiolabeled microsphere cerebral blood flow measurements in baboons. *Stroke* 1989;20:1716–1723
23. Gur D, Yonas H, Jackson DL, et al. Simultaneous measurements of cerebral blood flow by the xenon/CT method and the microsphere method. *Invest Radiol* 1985;20:672–677
24. Gur D, Yonas H, Jackson DL, et al. Measurement of cerebral blood flow during xenon inhalation as measured by the microspheres method. *Stroke* 1985;16:871–874
25. Drayer BP, Yonas H, Wolfson SK, Cook EE. Abnormality of the xenon brain:blood partition coefficient and blood flow in cerebral infarction: an *in vivo* assessment using transmission computed tomography. *Radiology* 1980;135:349–354
26. Fike J, Cann C, Berninger W. Quantitative evaluation of the canine brain using computed tomography. *J Comput Assist Tomogr* 1982;6:325–333
27. Hopper JL, Davis SM, Tress BM, Kaye AH, Rossiter SC, Derrick PL. Analysis of dynamic computed tomography scan brain images. *Invest Radiol* 1987;22:651–657
28. Klingensmith WC. Regional blood flow with first circulation time-indicator curves: a simplified, physiologic method of interpretation. *Radiology* 1983;149:281–286
29. Norman D, Axel L, Berninger WH, et al. Dynamic computed tomography of the brain: techniques, data analysis, and applications. *AJR: Am J Roentgenol* 1981;136:759–770
30. Boyd DP, Gould RG, Quinn JR, Stantey Y, Herrmansfeldt W. A proposed dynamic cardiac 3-D densitometer for early detection and evaluation of heart disease. *IEEE Trans Nucl Sci* 1979;26:2724
31. Tomita M, Gotoh F. Local cerebral blood flow values as estimated with diffusible tracers: validity of assumptions in normal and ischemic tissue. *J Cereb Blood Flow Metab* 1981;1:403–411
32. Hilal SK. Hemodynamic changes associated with the intra-arterial injection of contrast media. *Radiology* 1966;86:615–633
33. Nygren A, Ulfendahl HR, Hansell P, Erkison U. Effects of intravenous contrast media on cortical and medullary blood flow in the rat kidney. *Invest Radiol* 1988;23:753–761
34. Lacombe P, Meric P, Seylaz J. Validity of cerebral blood flow measurements obtained with quantitative tracer techniques. *Brain Res Rev* 1980;2:105–169
35. Gur D, Yonas H, Good WF. Local cerebral blood flow by xenon-enhanced CT: current status, potential improvements, and future directions. *Cerebrovasc Brain Metab Rev* 1989;1:68–86
36. Fike JR, Gobbel GT, Satoh T, Stauffer PR. Normal brain response after interstitial microwave hyperthermia. *Int J Hyperthermia* 1991;7:795–808
37. Gobbel GT, Seilhan TM, Fike JR. Cerebrovascular response after interstitial irradiation. *Radiat Res* 1992;130:236–240